

Silicon-based heterogeneous photonic integrated circuits for the mid-infrared

Gunther Roelkens,^{1,*} Utsav Dave¹, Alban Gassenq,¹ Nannicha Hattasan,¹ Chen Hu,¹ Bart Kuyken,¹ Francois Leo,¹ Aditya Malik,¹ Muhammad Muneeb,¹ Eva Ryckeboer,¹ Sarah Uvin¹, Zeger Hens,¹ Roel Baets,¹ Yosuke Shimura,² Federica Gencarelli,² Benjamin Vincent,² Roger Loo,² Joris Van Campenhout,² Laurent Cerutti,³ Jean-Baptiste Rodriguez,³ Eric Tournié,³ Xia Chen,⁴ Milos Nedeljkovic,⁴ Goran Mashanovich,⁴ Li Shen,⁴ Noel Healy,⁴ Anna C. Peacock,⁴ Xiaoping Liu,⁵ Richard Osgood,⁵ and William Green⁶

¹Photonics Research Group – Center for nano- and biophotonics (NB-Photonics), Sint-Pietersnieuwstraat 41, B-9000 Ghent, Belgium

²imec, Kapeldreef 75, B-3001 Leuven, Belgium

³Institut d'Electronique, UMR 5214, Université Montpellier 2 - CNRS, Montpellier, France

⁴Optoelectronics Research Centre, Faculty of Physical Sciences and Engineering, University of Southampton, Southampton, SO17 1BJ United Kingdom

⁵Department of Electrical Engineering, Columbia University, New York 10027, USA

⁶IBM T.J. Watson Research Center, 1101 Kitchawan Road, Yorktown Heights, New York 10598, USA

*gunther.roelkens@intec.ugent.be

Abstract: In this paper we present our recent work on mid-infrared photonic integrated circuits for spectroscopic sensing applications. We discuss the use of silicon-based photonic integrated circuits for this purpose and detail how a variety of optical functions in the mid-infrared besides passive waveguiding and filtering can be realized, either relying on nonlinear optics or on the integration of other materials such as GaSb-based compound semiconductors, GeSn epitaxy and PbS colloidal nanoparticles.

©2013 Optical Society of America

OCIS codes: (130.0130) Integrated optics.

References and links

1. Y. Vlasov, "Silicon integrated nanophotonics: road from scientific explorations to practical applications," plenary talk CLEO, United States, 2012.
2. K. De Vos, J. Molera, T. Claes, Y. De Koninck, S. Popelka, E. Schacht, R. Baets, and P. Bienstman, "Multiplexed antibody detection with an array of silicon-on-insulator microring resonators," *IEEE Photonics Journal* **1**(4), 225–235 (2009).
3. Y. Li and R. Baets, "Homodyne laser Doppler vibrometer on silicon-on-insulator with integrated 90 degree optical hybrids," *Opt. Express* **21**(11), 13342–13350 (2013).
4. J. G. Crowder, S. D. Smith, A. Vass, and J. Keddie, "Infrared methods for gas detection," in *Mid-infrared Semiconductor Optoelectronics* (Springer-Verlag, 2006).
5. H. Lin, L. Li, Y. Zou, S. Danto, J. D. Musgraves, K. Richardson, S. Kozacik, M. Murakowski, D. Prather, P. T. Lin, V. Singh, A. Agarwal, L. C. Kimerling, and J. Hu, "Demonstration of high-Q mid-infrared chalcogenide glass-on-silicon resonators," *Opt. Lett.* **38**(9), 1470–1472 (2013).
6. R. Shankar, I. Bulu, and M. Loncar, "Integrated high-quality factor silicon-on-sapphire ring resonators for the mid-infrared," *Appl. Phys. Lett.* **102**(5), 051108 (2013).
7. T. Baehr-Jones, A. Spott, R. Ilic, A. Spott, B. Penkov, W. Asher, and M. Hochberg, "Silicon-on-sapphire integrated waveguides for the mid-infrared," *Opt. Express* **18**(12), 12127–12135 (2010).
8. S. Khan, J. Chiles, J. Ma, and S. Fathpour, "Silicon-on-nitride waveguides for mid- and near-infrared integrated photonics," *Appl. Phys. Lett.* **102**(12), 121104 (2013).
9. P. T. Lin, V. Singh, L. Kimerling, and A. Agarwal, "Planar silicon nitride mid-infrared devices," *Appl. Phys. Lett.* **102**(25), 251121 (2013).
10. Z. Cheng, X. Chen, C. Y. Wong, K. Xu, and H. K. Tsang, "Mid-infrared suspended membrane waveguide and ring resonator on silicon-on-insulator," *IEEE Photonics Journal* **4**(5), 1510–1519 (2012).
11. G. Z. Mashanovich, M. M. Milošević, M. Nedeljkovic, N. Owens, B. Xiong, E. J. Teo, and Y. Hu, "Low loss silicon waveguides for the mid-infrared," *Opt. Express* **19**(8), 7112–7119 (2011).

12. P. T. Lin, V. Singh, Y. Cai, L. C. Kimerling, and A. Agarwal, "Air-clad silicon pedestal structures for broadband mid-infrared microphotronics," *Opt. Lett.* **38**(7), 1031–1033 (2013).
13. Y. C. Chang, V. Paeder, L. Hvozdar, J. M. Hartmann, and H. P. Herzig, "Low-loss germanium strip waveguides on silicon for the mid-infrared," *Opt. Lett.* **37**(14), 2883–2885 (2012).
14. R. Soref, "Mid-infrared photonics in silicon and germanium," *Nat. Photonics* **4**(8), 495–497 (2010).
15. N. Hattasan, B. Kuyken, F. Leo, E. Ryckeboer, D. Vermeulen, and G. Roelkens, "High-efficiency SOI fiber-to-chip grating couplers and low-loss waveguides for the short-wave infrared," *IEEE Photon. Technol. Lett.* **24**(17), 1536–1538 (2012).
16. F. Leo, B. Kuyken, N. Hattasan, R. Baets, and G. Roelkens, "Passive SOI devices for the short-wave infrared," *European Conference on Integrated Optics (ECIO 2012)*, 156–158, Spain (2012).
17. E. Ryckeboer, A. Gassenq, M. Muneeb, N. Hattasan, S. Pathak, L. Cerutti, J.-B. Rodriguez, E. Tournié, W. Bogaerts, R. Baets, and G. Roelkens, "Silicon-on-insulator spectrometers with integrated GaInAsSb photodiodes for wide-band spectroscopy from 1510 to 2300 nm," *Opt. Express* **21**(5), 6101–6108 (2013).
18. M. Muneeb, X. Chen, P. Verheyen, G. Lepage, S. Pathak, E. Ryckeboer, A. Malik, B. Kuyken, M. Nedeljkovic, J. Van Campenhout, G. Z. Mashanovich, and G. Roelkens, "Demonstration of Silicon-on-insulator mid-infrared spectrometers operating at 3.8 μm ," *Opt. Express* **21**(10), 11659–11669 (2013).
19. A. Malik, M. Muneeb, Y. Shimura, J. Van Campenhout, G. Roelkens, "Germanium-on-silicon mid-infrared waveguides and Mach-Zehnder interferometers," accepted for publication in *IEEE Photonics Conference* (2013).
20. L. Zhang, Q. Lin, Y. Yue, Y. Yan, R. Beausoleil, A. Agarwal, L. Kimerling, J. Michel, and A. Willner, "On-chip octave-spanning supercontinuum in nanostructured silicon waveguides using ultralow pulse energy," *Journal of Sel. Topics in Quantum Electronics* **18**(6), 1799–1806 (2012).
21. G. P. Agrawal, "*Nonlinear Fiber Optics*," 195–211 (Springer Berlin Heidelberg, 2006).
22. B. Kuyken, X. Liu, G. Roelkens, R. Baets, R. M. Osgood, Jr., and W. M. J. Green, "50 dB parametric on-chip gain in silicon photonic wires," *Opt. Lett.* **36**(22), 4401–4403 (2011).
23. B. Kuyken, X. Liu, R. M. Osgood, Jr., R. Baets, G. Roelkens, and W. M. J. Green, "Mid-infrared to telecom-band supercontinuum generation in highly nonlinear silicon-on-insulator wire waveguides," *Opt. Express* **19**(21), 20172–20181 (2011).
24. B. Kuyken, X. Liu, R. M. Osgood, Jr., R. Baets, G. Roelkens, and W. M. J. Green, "A silicon-based widely tunable short-wave infrared optical parametric oscillator," *Opt. Express* **21**(5), 5931–5940 (2013).
25. X. Liu, B. Kuyken, G. Roelkens, R. Baets, R. M. Osgood, Jr., and W. M. J. Green, "Bridging the mid-infrared-to-telecom gap with silicon nanophotonic spectral translation," *Nat. Photonics* **6**(10), 667–671 (2012).
26. M. Lamont, R. Lau, A. Griffith, Y. Wen, Y. Okawachi, M. Lipson, and A. Gaeta, "Mid-infrared supercontinuum generation in silicon waveguides," *CLEO, CW3H.1*, United States (2013).
27. B. Kuyken, P. Verheyen, P. Tannouri, J. Van Campenhout, R. Baets, G. Roelkens, and W. M. J. Green, "Mid-infrared generation by frequency down-conversion across 1.2 octaves in a normally-dispersive silicon wire," *CLEO, CTh1F.2*, United States, 2013.
28. B. Kuyken, S. Clemmen, S. K. Selvaraja, W. Bogaerts, D. Van Thourhout, Ph. Emplit, S. Massar, G. Roelkens, and R. Baets, "On-chip parametric amplification with 26.5 dB gain at telecommunication wavelengths using CMOS-compatible hydrogenated amorphous silicon waveguides," *Opt. Lett.* **36**(4), 552–554 (2011).
29. D. L. Staebler and C. R. Wronski, "Reversible conductivity changes in discharge-produced amorphous Si," *Appl. Phys. Lett.* **31**(4), 292–295 (1977).
30. S. Uvin, U. Dave, B. Kuyken, S. Selvaraja, F. Leo, and G. Roelkens, "Mid-infrared to telecom-band stable supercontinuum generation in hydrogenated amorphous silicon waveguides," accepted for publication in *IEEE Photonics Conference*, United States, 2013.
31. K. Wang, M. Foster, and A. Foster, "Wavelength-agile near-infrared chip-based optical parametric oscillator using a deposited silicon waveguide," *CLEO, CTh5D*, United States, 2013.
32. N. Hon, R. Soref, and B. Jalali, "The third-order nonlinear optical coefficients of Si, Ge, and SiGe in the midwave and longwave infrared," *J. Appl. Phys.* **110**(1), 011301 (2011).
33. D. Ahn, C. Y. Hong, J. Liu, W. Giziewicz, M. Beals, L. C. Kimerling, J. Michel, J. Chen, and F. X. Kärtner, "High performance, waveguide integrated Ge photodetectors," *Opt. Express* **15**(7), 3916–3921 (2007).
34. L. Vivien, J. Osmond, J. M. Fédéli, D. Marris-Morini, P. Crozat, J. F. Damlencourt, E. Cassan, Y. Lecunff, and S. Laval, "42 GHz p-i-n germanium photodetector integrated in a silicon-on-insulator waveguide," *Opt. Express* **17**(8), 6252–6257 (2009).
35. R. E. Camacho-Aguilera, Y. Cai, N. Patel, J. T. Bessette, M. Romagnoli, L. C. Kimerling, and J. Michel, "An electrically pumped germanium laser," *Opt. Express* **20**(10), 11316–11320 (2012).
36. G. Sun, R. A. Soref, and H. H. Cheng, "Design of a Si-based lattice-matched room-temperature GeSn/GeSiSn multi-quantum-well mid-infrared laser diode," *Opt. Express* **18**(19), 19957–19965 (2010).
37. R. Roucka, J. Xie, J. Kouvetakis, J. Mathews, V. D'Costa, J. Menendez, J. Tolle, and S. Qu, "GeSn photoconductor structures at 1.55 μm : from advanced materials to prototype devices," *J. Vac. Sci. Technol.* **26**(6), 1952–1955 (2008).
38. S. Su, B. Cheng, C. Xue, W. Wang, Q. Cao, H. Xue, W. Hu, G. Zhang, Y. Zuo, and Q. Wang, "GeSn p-i-n photodetector for all telecommunication bands detection," *Opt. Express* **19**(7), 6400–6405 (2011).
39. A. Gassenq, F. Gencarelli, J. Van Campenhout, Y. Shimura, R. Loo, G. Narcy, B. Vincent, and G. Roelkens, "GeSn/Ge heterostructure short-wave infrared photodetectors on silicon," *Opt. Express* **20**(25), 27297–27303 (2012).

40. G. Roelkens, L. Liu, D. Liang, R. Jones, A. Fang, B. Koch, J. Bowers, "III-V/silicon photonics for on-chip and inter-chip optical interconnects," *Laser & Photonics Reviews*, p.DOI: 10.1002/lpor.200900033 (2010)
41. N. Hattasan, A. Gassenq, L. Cerutti, J. B. Rodriguez, E. Tournié, and G. Roelkens, "Heterogeneous integration of GaInAsSb p-i-n photodiodes on a silicon-on-insulator waveguide circuit," *IEEE Photon. Technol. Lett.* **23**(23), 1760–1762 (2011).
42. A. Gassenq, N. Hattasan, L. Cerutti, J. B. Rodriguez, E. Tournié, G. Roelkens, and G. Roelkens, "Study of evanescently-coupled and grating-assisted GaInAsSb photodiodes integrated on a silicon photonic chip," *Opt. Express* **20**(11), 11665–11672 (2012).
43. L. Cerutti, J. B. Rodriguez, and E. Tournie, "GaSb-based laser, monolithically grown on silicon substrate, emitting at 1.55 μ m at room temperature," *IEEE Photon. Technol. Lett.* **22**(8), 553–555 (2010).
44. J. B. Rodriguez, L. Cerutti, P. Grech, and E. Tournié, "Room-temperature operation of a 2.25 μ m electrically pumped laser fabricated on a silicon substrate," *Appl. Phys. Lett.* **94**(6), 061124 (2009).
45. C. Tsay, F. Toor, C. F. Gmachl, and C. B. Arnold, "Chalcogenide glass waveguides integrated with quantum cascade lasers for on-chip mid-IR photonic circuits," *Opt. Lett.* **35**(20), 3324–3326 (2010).
46. J. Wang, T. Zens, J. Hu, P. Becla, L. Kimerling, and A. Agarwal, "Monolithically integrated, resonant-cavity-enhanced dual-band mid-infrared photodetector on silicon," *Appl. Phys. Lett.* **100**(21), 211106 (2012).
47. T. Zens, P. Becla, A. Agarwal, L. Kimerling, and A. Drehman, "Long wavelength infrared detection using amorphous InSb and InAsSb," *J. Cryst. Growth* **334**, 84–89 (2011).
48. Y. Zhang, T. Liu, B. Meng, X. Li, G. Liang, X. Hu, and Q. J. Wang, "Broadband high photoresponse from pure monolayer graphene photodetector," *Nat. Communications* DOI: 10.1038/ncomms2830 (2013)
49. C. Hu, A. Gassenq, Y. Justo, Z. Hens, and G. Roelkens, Colloidal quantum dot photodetectors on silicon for short-wave infrared applications," *E-MRS 2013 Spring Meeting, France* (2013).
50. I. Moreels, K. Lambert, D. Smeets, D. De Muynck, T. Nollet, J. C. Martins, F. Vanhaecke, A. Vantomme, C. Delerue, G. Allan, and Z. Hens, "Size-dependent optical properties of colloidal PbS quantum Dots," *ACS Nano* **3**(10), 3023–3030 (2009).
51. A. Nag, M. V. Kovalenko, J. S. Lee, W. Liu, B. Spokoyny, and D. V. Talapin, "Metal-free inorganic ligands for colloidal nanocrystals: S²⁻, HS⁻, Se²⁻, HSe⁻, Te²⁻, HTe⁻, TeS₃²⁻, OH⁻, and NH₂⁻ as surface ligands," *J. Am. Chem. Soc.* **133**(27), 10612–10620 (2011).
52. S. Keuleyan, E. Lhuillier, V. Brajuskovic, and P. Guyot-Sionnest, "Mid-infrared HgTe colloidal quantum dot photodetectors," *Nat. Photonics* **5**(8), 489–493 (2011).
53. N. MacSuihbne, Z. Li, B. Baeuerle, J. Zhao, J. Wooller, S. Alam, F. Poletti, M. Petrovich, A. Heidt, I. Giles, D. Giles, B. Palsdottir, J. Gruner-Nielsen, R. Phelan, J. O'Carroll, B. Kelly, D. Murphy, A. Ellis, D. Richardson, and F. Garcia Gunning, "Wavelength division multiplexing at 2 μ m," *European Conference on Optical Communication, PDP Th3A3* (2012)

1. Introduction

Silicon photonics is emerging as a key enabling technology for the realization of highly integrated photonic circuits. While originally conceived for datacom and telecom applications [1], the scope of potential applications has in recent years broadened to the use of silicon photonic integrated circuits for sensing [2] and biomedical instrumentation [3]. However, in these applications one typically retains the telecommunication wavelength range (1.3–1.55 μ m) for implementing these functions. On the other hand, stepping away from this wavelength range, particularly in the field of optical sensing, could enable a whole new class of devices with unprecedented sensitivity and selectivity by exploiting the very specific and strong absorption features of molecules in the mid-infrared (2–8 μ m) [4]. Such spectroscopic sensing systems are envisioned for use in handheld applications, requiring a compact, rugged and low power consumption solution, which make an integrated approach very attractive. Therefore, in this paper we will elaborate on the technological developments and demonstrations that we have recently achieved in the field of silicon-based mid-infrared photonic integrated circuits and devices, and relate these developments to their impact on chip-scale sensing. The paper is organized as follows: in Section 2, mid-IR passive silicon-based waveguide circuits are presented, Section 3 deals with the use of these waveguide structures for nonlinear optics based mid-infrared light generation (parametric amplification, parametric oscillation and supercontinuum generation) and upconversion, while Sections 4 to 6 deal with the integration of materials (GaSb-based compound semiconductors, GeSn epitaxy and PbS colloidal nanoparticles) on top of the silicon waveguide circuit to complement the functionality that can be realized purely in silicon.

2. Passive silicon-based waveguide circuits for the mid-infrared

Several waveguide platforms have been proposed in recent years for mid-infrared photonics, including chalcogenide glass-based circuits [5], silicon-on-sapphire [6,7] and silicon-on-siliconnitride [8], siliconnitride/SiO₂ waveguides [9], suspended silicon waveguides [10], porous silicon waveguides [11], silicon pedestal waveguides [12] and germanium-on-silicon waveguide structures [13], each with their own advantages and drawbacks. Silicon photonic integrated circuits for the telecommunication wavelength window are typically realized on silicon-on-insulator wafers, due to the high refractive index contrast between the silicon core and SiO₂ or air cladding that is available on this platform. This contrast allows realization of compact photonic integrated circuits leveraging the well-developed CMOS fabrication infrastructure. Therefore, it makes sense to evaluate how far the wavelength range of operation can be pushed into the infrared using such a platform. While silicon itself is transparent up to a wavelength of about 8 μ m wavelength, the SiO₂ buried oxide layer starts to absorb heavily at a wavelength of about 4 μ m, thereby limiting the silicon-on-insulator transparency range from 1.1 to 4 μ m [14]. Moreover, care should be taken that the SiO₂ buried oxide layer thickness be sufficiently thick to avoid substantial substrate leakage, especially at longer wavelengths. SOI wafers with a 220nm thick silicon device layer have emerged as a relatively common standard for telecommunication wavelength range applications. Therefore, in order to exploit as much as possible the existing technology base, waveguide circuits for the short-wave infrared (2-2.5 μ m) can best be implemented on this platform. For longer wavelengths the silicon device layer thickness becomes too thin and thicker waveguide layers should be used. On the 220nm SOI platform several basic passive optical components have been realized for the 2-2.5 μ m wavelength range, which can now be used in a spectroscopic sensing system. These include high index contrast waveguides with low optical loss (0.5dB/cm) [15], high efficiency (3.8dB insertion loss) fiber-to-chip grating couplers [15], ring resonators with a Q-factor of 10⁵ [16] and wavelength (de)multiplexers based on arrayed waveguide gratings and *echelle* gratings [17]. Performance metrics representative of these different devices are shown in Fig. 1. Figure 1(a) shows the optical waveguide loss of a 900nm wide and 220nm high air clad silicon wire in the 2.1 to 2.3 μ m wavelength range for the fundamental TE mode. The TE polarization fiber-to-chip coupling spectrum (using standard single mode fiber SMF-28) of a silicon grating coupler structure is shown in Fig. 1(b), illustrating a 90nm 3dB bandwidth. The through port spectrum of a high-Q ring resonator implemented on this platform is shown in Fig. 1(c), while Fig. 1(d) shows the spectral response of a 6 channel arrayed waveguide grating wavelength demultiplexer. All of these components are fabricated using standard CMOS fabrication technology on 200mm SOI wafers, alongside photonic integrated circuits for the telecommunication window.

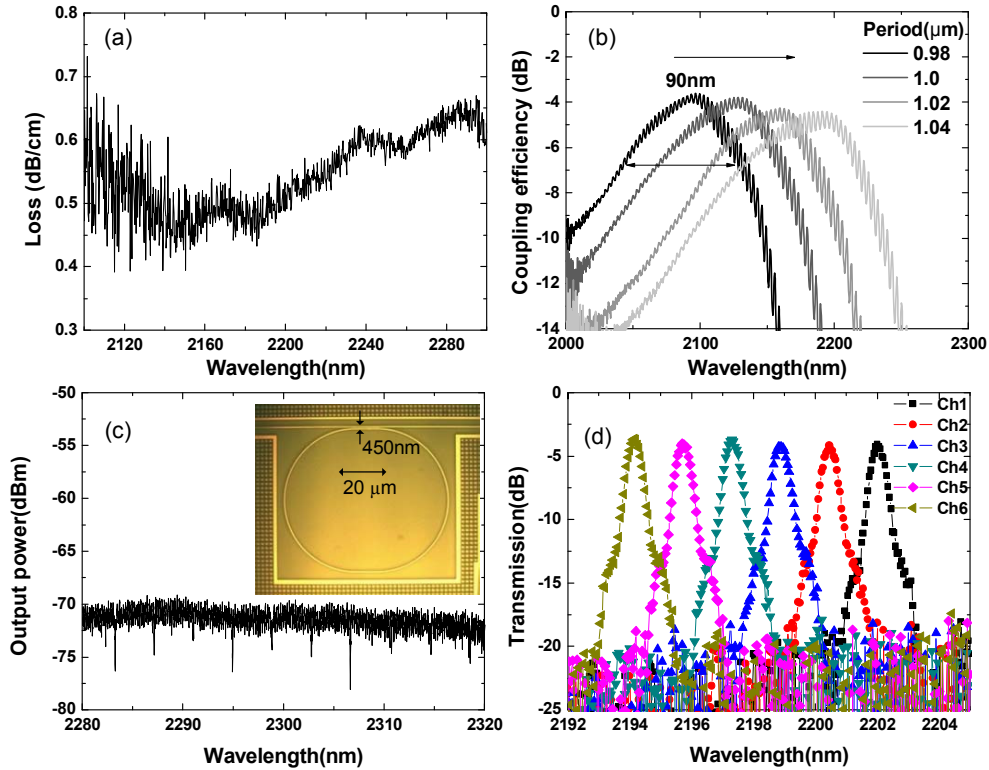


Fig. 1. (a) Waveguide loss as a function of wavelength for a 900nm by 220nm air clad single mode silicon waveguide (fundamental TE mode); (b) fiber-to-chip grating coupler efficiency spectrum for TE polarized light; (c) transmission spectrum of an all-pass ring resonator in the 2.3 μ m wavelength range; (d) wavelength (de)multiplexing characteristic of an arrayed waveguide grating device.

While the 220nm thick silicon waveguide platform already allows implementing several optical functions with good performance, a larger flexibility in device geometry can be obtained if an additional layer of poly-silicon can locally be added on top of the 220nm silicon device layer. This is, for example, the case for the fiber-to-chip grating coupler that was discussed above [15]. Moreover, the availability of a thicker silicon device layer permits extension of the wavelength range of operation to the 4 μ m wavelength transparency edge of the SOI platform. This extension was demonstrated in [18] where we realized low-loss silicon waveguides operating at a wavelength of 3.8 μ m wavelength, as well as high-performance wavelength (de)multiplexer circuits, as shown in Fig. 2. While the losses at 3.8 μ m on the 220nm crystalline silicon / 160nm poly-crystalline silicon platform for a 1.45 μ m wide single mode waveguide are around 6dB/cm (WG2), better performance can be obtained with a fully crystalline Si device layer, since the Rayleigh scattering losses in the poly-crystalline silicon can be avoided. For example, propagation losses in the range of 3-4dB/cm are obtained for a 1.45 μ m wide, 400nm high crystalline silicon waveguide (WG1).

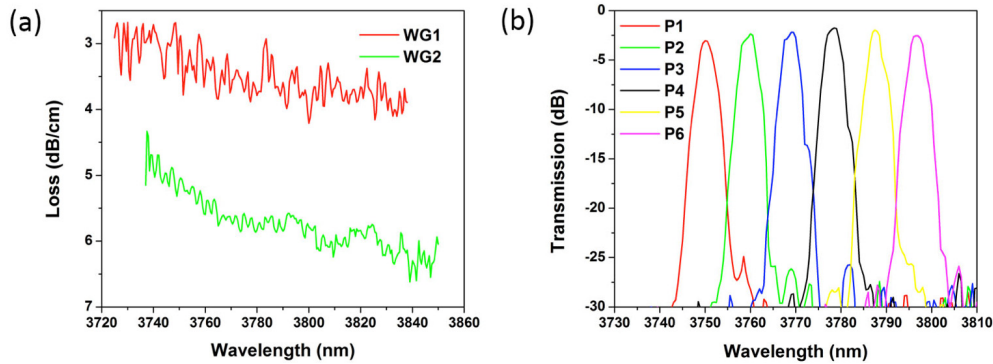


Fig. 2. (a) Silicon-on-insulator waveguide losses in the 3.8 μ m wavelength range for 400nm c-Si waveguide layers (WG1) and 220nm c-Si/160nm p-Si (WG2); (b) example of an arrayed waveguide grating wavelength demultiplexer operating at 3.8 μ m implemented on the 220nm c-Si/160nm p-Si platform.

Beyond a wavelength of 4 μ m, alternative silicon-based waveguide platforms need to be explored. Several approaches can be followed. Silicon-on-sapphire waveguide circuits can be used, which still exploit the high refractive index contrast between the silicon waveguide core and the sapphire substrate [6,7]. The transparency window in this case is limited to about 5.5 μ m wavelength, matching that of sapphire. An alternative is the use of free-standing silicon waveguide structures [10] and silicon pedestal waveguides [12], allowing the use of the full transparency window of silicon up to a wavelength of 8 μ m wavelength. Such an approach is however less flexible with respect to the types of devices that can be made, given the sideways underetching required by such structures. Another platform that can be used is germanium on silicon [13]. Since the epitaxial growth of germanium on silicon is well mastered both for optical and electronic applications, Ge films of high quality can be used as the waveguide core, despite the large lattice constant mismatch between germanium and silicon. Given the broad transparency range of germanium in the infrared (up to 14 μ m) this appears to be a very attractive solution for photonic integrated circuits operating beyond 4 μ m wavelength. Recently we have demonstrated 3dB/cm waveguide losses in the 5-5.5 μ m wavelength range on this platform. In addition, we have realized basic optical components such as Mach-Zehnder interferometers (as shown in Fig. 3 [19]), which can be used, for example, in the wavelength multiplexing of arrays of quantum cascade DFB lasers.

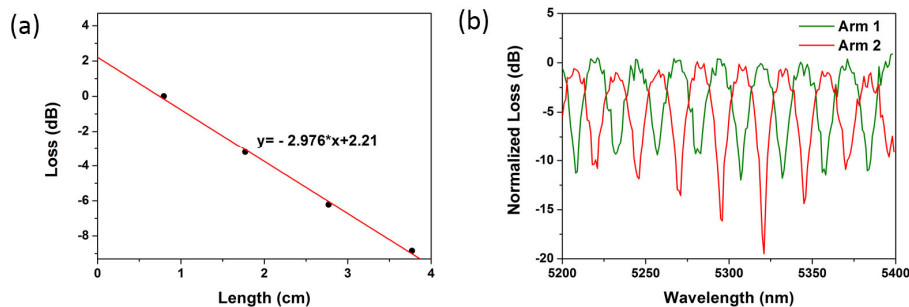


Fig. 3. (a) Ge-on-Si waveguide normalized losses at 5 μ m wavelength for a 2 μ m thick germanium device layer thickness (2.2 μ m waveguide width, completely etched through the germanium waveguide core). (b) Mach-Zehnder interferometer implemented in Ge on Si for wavelength multiplexing purposes.

3. Nonlinear optics on a silicon photonics platform at mid-infrared wavelengths

3.1 Introduction

While silicon photonics provides a good platform for the implementation of passive linear waveguide circuits, such as elaborated on in Section 2, an even broader range of novel functionalities can be implemented on a chip when one exploits the strong nonlinear response of high index contrast silicon photonic waveguides. This possibility was already recognized for telecommunication applications, given the tight confinement in a sub-micron size silicon waveguide and the intrinsically high Kerr nonlinearity of silicon. However, the performance of such silicon devices in the telecommunication wavelength range is severely limited due to parasitic two-photon absorption. A major advantage of working at longer wavelengths, specifically in the 2-2.5 μm wavelength range, is that two-photon absorption and its associated free carrier absorption can be substantially reduced, making silicon photonic waveguide circuits ideal for the implementation of nonlinear optical functions. In the subsequent sections we will elaborate on nonlinear functionalities that have been implemented in the short-wave infrared (2-2.5 μm), both in crystalline and hydrogenated amorphous silicon. We also present platform options for operation beyond 4 μm .

3.2 Nonlinear optics in crystalline silicon-on-insulator

The strong third order nonlinearity of silicon, combined with the tight optical confinement, the large freedom in dispersion engineering of silicon photonic wire waveguides [20] and the absence of parasitic two-photon absorption above 2.2 μm makes silicon-on-insulator waveguide structures ideal for implementing four-wave-mixing based nonlinear functions. When a high intensity electromagnetic wave is present in a third-order nonlinear medium, a process called modulation instability can occur [21]; this process relates to the parametric amplification of background noise in wavelength bands around the pump (a signal wavelength band on the short wavelength side and an idler wavelength band on the long wavelength side of the pump). The exact position (and the mere occurrence of such parametric amplification) is determined by the dispersion of the silicon photonic waveguide. Efficient parametric amplification will occur when

$$\Delta k_{\text{lin}} + 2\gamma P = 0, \quad (1)$$

in which Δk_{lin} is the linear phase mismatch between the signal, idler and pump wave ($\Delta k_{\text{lin}} = k_s + k_i - 2k_p$). $2\gamma P$ is the nonlinear phase mismatch term, in which P is the (peak) power of the pump beam in the silicon waveguide and γ is the nonlinear parameter of the silicon waveguide ($\gamma = n_2 \omega / A_{\text{eff}} c$, with n_2 the nonlinear refractive index and A_{eff} the effective waveguide cross-section). Equation (1) can be rewritten by considering the Taylor expansion of the waveguide dispersion relation $k(\omega)$ around the pump wavelength

$$k(\omega) = k(\omega_p) + \beta_1(\omega - \omega_p) + \frac{1}{2}\beta_2(\omega - \omega_p)^2 + \dots, \quad (2)$$

with $\beta_i \triangleq \left. \frac{d^i k}{d\omega^i} \right|_{\omega=\omega_p}$. By making use of the fact that $\omega_s - \omega_p = \omega_p - \omega_i = \Omega$ due to energy conservation, we can rewrite Eq. (1) up to fourth order as

$$\beta_2 \Omega^2 + \frac{1}{12} \beta_4 \Omega^4 + 2\gamma P = 0. \quad (3)$$

From this phase matching condition several conclusions can be drawn. For the case in which we consider parametric amplification close to the pump, the fourth-order term can be neglected. Therefore, $\beta_2 < 0$ is required to obtain phase matching. This condition implies that

the waveguide must show anomalous group velocity dispersion. Alternatively, when considering wavelength bands far away from the pump the fourth-order term needs to be taken into account. In order to have a solution far away from the pump (large Ω), β_2 and β_4 must therefore be of opposite sign. In the case $\beta_2 < 0$ and $\beta_4 > 0$, both a wavelength band close to the pump (broadband modulation instability) and far away from the pump (narrowband modulation instability) will experience parametric amplification, while in the opposite case ($\beta_2 > 0$ and $\beta_4 < 0$) only narrow band modulation instability far away from the pump will be observed. These conditions are schematically illustrated in Fig. 4.

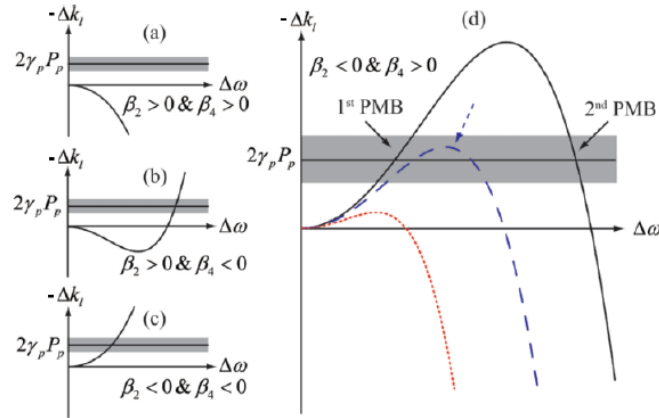


Fig. 4. The phase mismatch as a function of detuning frequency from the pump. Depending on the sign of β_2 and β_4 the phase matching equations have several solutions (PMB = phase matching band).

Several device demonstrations have been recently realized in silicon photonic waveguide circuits based on parametric amplification due to a strong pump wave in the 2.x μm wavelength range. These include the demonstration of >50dB (Raman assisted) parametric gain in a 2cm long silicon photonic wire waveguide (900nm wide, 220nm thick silicon waveguide core) [22], the generation of a 1.5 μm to 2.5 μm spanning supercontinuum [23], and a fiber loop based tunable optical parametric oscillator based on a silicon photonic wire parametric gain element [24]. Narrowband parametric amplification was shown in [25], where the downconversion of a telecom-band signal to the mid-infrared and the upconversion of such a mid-infrared signal to the telecom band were demonstrated. These demonstrations show the promise of nonlinear silicon photonic integrated circuits, since these processes can facilitate the generation and detection of mid-infrared signals based on mature telecom-band sources and detectors respectively.

These key results are summarized in Fig. 5. In all these experiments a 2.x μm picosecond pulse train with a 76MHz repetition rate generated by a Coherent/MIRA OPO system was used as the pump. Figure 5(a) shows the measured parametric amplification of a continuous wave probe laser in the presence of a 13.5W peak power pulse train at 2.175 μm wavelength in a 900nm wide by 220nm high waveguide (2cm length). A maximum Raman-assisted gain peak of greater than 50dB can be observed. Figure 5(b) shows the generation of a mid-infrared to telecom-band supercontinuum in similar 2cm long waveguides; this continuum results from the complex interplay between modulation instability, self-phase modulation, Raman amplification, cascaded four-wave mixing, and dispersive wave generation. The four different spectra (from bottom to top) correspond to a 3.1 W, 4.3 W, 7.9 W and 12.7 W peak power pulse train at 2120nm on the chip. Recently, a femtosecond pulsed laser source was used to generate an octave-spanning soliton-fission driven mid-infrared supercontinuum in a silicon-on-insulator waveguide [26]. Figure 5(c) shows the tuning characteristic of a

synchronously pumped optical parametric oscillator using a silicon photonic wire as the nonlinear gain medium. By adjusting the delay in the fiber feedback loop, wavelength tuning could be realized due to the fiber dispersion. Figure 5(d) illustrates the use of discrete band modulation instability to upconvert a 2.44 μm continuous wave signal into the telecommunication wavelength range using four-wave mixing with a pump at 1946nm. This spectral translation enables the detection of mid-infrared radiation using high sensitivity telecom photodetectors operating at room temperature. Using the same four-wave mixing process, mid-infrared radiation can also be generated in this manner, by downconversion of telecommunication wavelength range (tunable) laser sources.

To illustrate the large degree of freedom in dispersion engineering and to facilitate confinement of longer-wavelength idler radiation in the silicon waveguide, narrowband parametric amplifiers in SOI waveguides 400nm thick and 1650 nm wide were recently demonstrated. The results showed octave spanning four-wave-mixing and the generation of 3.6 μm radiation with a 2.19 μm pump [27].

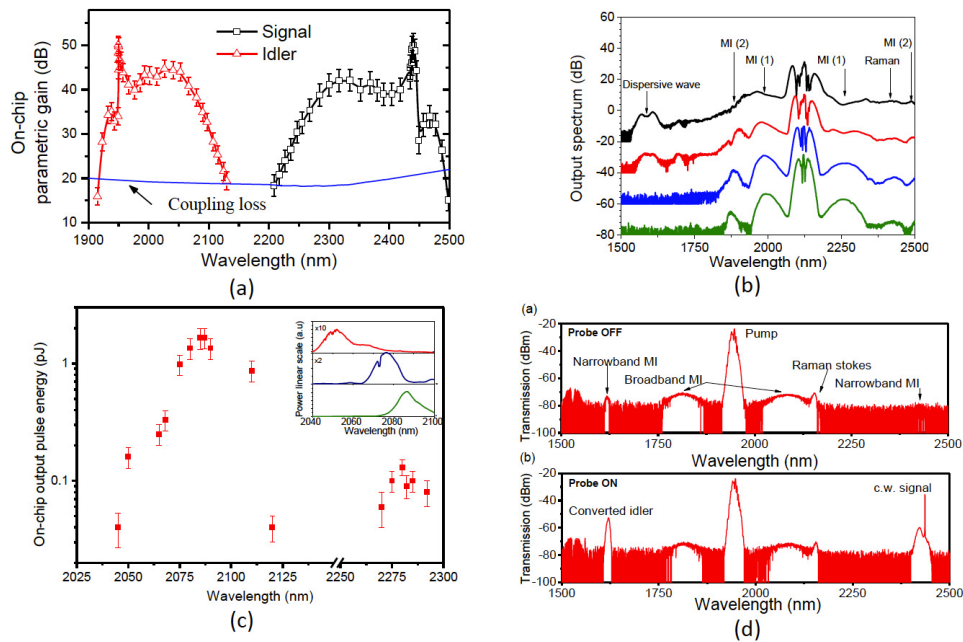


Fig. 5. (a) Greater than 50dB Raman assisted parametric amplification in wavelength bands close to the 2.175 μm pump wavelength; (b) supercontinuum generation in a silicon waveguide due to the complex interplay of modulation instability, self-phase modulation, Raman amplification, cascaded four wave mixing and dispersive wave generation; (c) tuning characteristic of a fiber loop based tunable optical parametric oscillator based on a silicon parametric gain chip; (d) spectral translation between the telecom and mid-infrared wavelength band.

3.3 Nonlinear optics in hydrogenated amorphous silicon

The use of crystalline silicon in the short-wave infrared allows for efficient nonlinear optical processes based on parametric amplification. However, in order to avoid parasitic two-photon absorption a pump wavelength longer than 2.2 μm is required. Such a pump requires the use of bulky optical pump sources such as the OPO system used in the previous experiments. In order to make more compact systems, it would be beneficial to be able to exploit the recently developed Thulium doped fiber lasers and amplifiers operating in the 1.9-2.0 μm wavelength range. However, this wavelength would still result in substantial two-photon absorption in

crystalline silicon waveguides. Therefore the use of hydrogenated amorphous silicon waveguide structures was evaluated, given the larger bandgap of hydrogenated amorphous silicon with respect to crystalline silicon waveguides. The use of hydrogenated amorphous silicon for third order nonlinear optics applications was demonstrated previously in the telecommunication wavelength band, showing a substantially higher nonlinearity and lower two-photon absorption compared to crystalline silicon [28]. However, the material was proven to be unstable under prolonged exposure to the high intensity pump. This was attributed to the Staebler-Wronski effect [29] (well known for amorphous silicon solar cells), in which electron-hole pairs generated in the material recombine close to a weak Si-Si bond, thus resulting in the breaking of the Si-Si bond and hence in a degradation of the material. However, by operating at the Thulium fiber source wavelength range, no strong parasitic two-photon absorption – and hence electron-hole pair generation – is to be expected in hydrogenated amorphous silicon. This was recently demonstrated by showing the generation of a supercontinuum in an air-clad a-Si waveguide (900nm wide, 220nm high) using a Thulium fiber laser picosecond pulse source, without observable degradation of the material over time, as shown in Fig. 6 [30]. This provides scope for the implementation of compact integrated mid-infrared optical systems based on nonlinear hydrogenated amorphous silicon waveguide structures. Recently, it was also demonstrated that hydrogenated amorphous silicon waveguides can be stable at 1550nm wavelength [31], even further widening the scope of applications for this material platform.

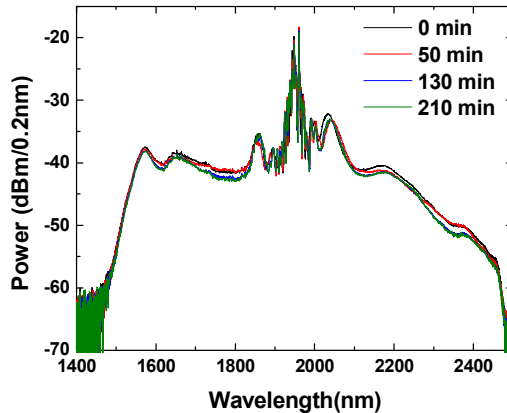


Fig. 6. Generation of a supercontinuum in an amorphous silicon waveguide using a Thulium fiber picosecond pulse source at 1950nm wavelength. No degradation of the a-Si can be observed.

3.3 Nonlinear optics beyond 4 μm wavelength

Since silicon-on-insulator waveguide circuits absorb heavily beyond 4 μm wavelength, other waveguide platforms need to be explored for nonlinear optical circuits in this wavelength range. While free-standing silicon waveguide circuits, silicon-on-sapphire waveguide circuits, silicon pedestal waveguide circuits and silicon-on-siliconnitride waveguide circuits provide a high refractive index contrast which lends itself to efficient nonlinear optical circuits, also germanium-on-silicon should be considered for this purpose, given the very broad transparency range of germanium and the larger Kerr nonlinearity in germanium compared to silicon [32].

4. Monolithically integrated devices

While the passive silicon structures described above provide an excellent platform for mid-IR waveguides, spectral filters and nonlinear optics, there is a need for other integrated components such as mid-infrared photodetectors and laser sources integrated onto the

platform. This can be realized in several ways. A very attractive approach in view of cost would be to monolithically integrate such opto-electronic devices onto the silicon platform. Germanium-based materials can be used for this purpose. While Ge photodetectors [33,34] and lasers [35] have been demonstrated on the silicon platform, the bandgap of Ge restricts their use to the telecommunication wavelength band. To extend the operational wavelength range to the mid-infrared, Sn can be added to the germanium matrix in order to reduce its bandgap. Moreover it turns out that adding Sn to the matrix makes the bandgap more direct, providing scope for the realization of group IV-based lasers on the silicon platform [36]. GeSn p-i-n photodetectors and photoconductors with improved response compared to germanium detectors at a wavelength of 1550nm have been demonstrated [37,38]. In order to demonstrate the potential of GeSn-based opto-electronic devices, a $\text{Ge}_{0.9}\text{Sn}_{0.1}$ three quantum well structure sandwiched between Ge cladding layers was grown by MOCVD on 200mm silicon wafers and photoconductor operation up to 2.5 μm wavelength was demonstrated. This is illustrated in Fig. 7(a) [39] showing the responsivity of surface illuminated $\text{Ge}_{0.9}\text{Sn}_{0.1}/\text{Ge}$ photoconductors as a function of wavelength and as a function of the number of $\text{Ge}_{0.9}\text{Sn}_{0.1}$ quantum wells. Given the compatibility of this epitaxial growth process with selective area growth, GeSn-based photodetectors integrated with passive silicon waveguide circuitry (e.g. implementing a wavelength demultiplexing functionality) can immediately be envisioned. Also germanium-on-silicon waveguide circuits with monolithically integrated GeSn detectors can be envisioned, given the fact that a Ge buffer layer is grown on the silicon substrate for the GeSn growth, which can act as a waveguide layer in the 2-2.5 μm wavelength range, where the GeSn detectors are sensitive. In order to evaluate the feasibility of such a platform, the propagation losses of a 2.25 μm wide and 1 μm thick germanium waveguide was evaluated in the short-wave infrared, as shown in Fig. 7(b). These low losses indicate that such a platform can be envisioned for the realization of monolithically integrated short-wave infrared spectrometers.

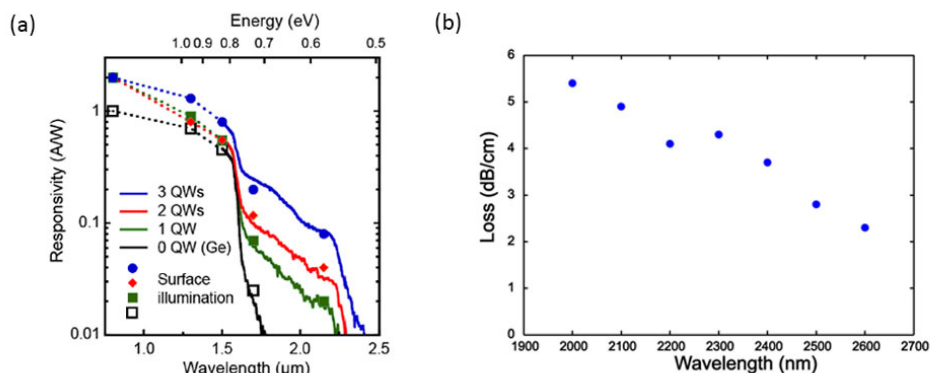


Fig. 7. (a) GeSn/Ge photoconductor integrated on a 200mm silicon wafer demonstrating the potential of GeSn heterostructures for the realization of mid-infrared opto-electronic devices on silicon photonic integrated circuits: responsivity as a function of wavelength and as a function of the number of GeSn quantum wells; (b) germanium-on-silicon waveguide losses in the short wave infrared (2.25 μm wide and 1 μm thick germanium waveguide).

5. Heterogeneously integrated III-V on silicon devices and systems

An alternate approach to integrating mid-IR opto-electronic components on the silicon waveguide platform is by the heterogeneous integration of III-V semiconductor device stacks onto the silicon waveguide circuits. This heterogeneous integration process is by now a well-developed technology for the transfer of InP-based epitaxy onto silicon waveguide circuits, in order to realize integrated laser sources, amplifiers, modulators and photodetectors operating

at telecommunication wavelengths [40]. While the emission wavelength of InP-based epitaxy using band-to-band optical transitions can be stretched to approximately $2.2\mu\text{m}$, and for photodetectors to a cut-off wavelength of about $2.6\mu\text{m}$ using extended InGaAs, a more flexible and further-reaching approach would be to integrate GaSb-based epitaxy on the silicon platform, allowing operation in the 2-3.5 μm wavelength range. The use of superlattice structures can permit extending the wavelength range of operation even further into the infrared. Therefore, a GaSb-to-silicon heterogeneous integration process was developed based on DVS-BCB adhesive wafer bonding. This process uses the commercial polymer DVS-BCB as an adhesive bonding agent between the silicon waveguide circuit wafer and the III-V material, which is bonded epi-side down to the silicon wafer, after which the GaSb growth substrate is removed by mechanical grinding and wet chemical etching, leaving the GaSb epitaxial film attached to the silicon waveguide circuit. This epitaxial layer can then be processed into an integrated photodetector or laser coupled to the silicon waveguide circuit.

The heterogeneous integration of GaSb photodetectors with silicon waveguide circuits based on this process was recently demonstrated [41,42]. Photodetectors with a cut-off wavelength of $2.5\mu\text{m}$ and a responsivity above 1A/W were demonstrated. The integration of an array of such photodetectors on a silicon spectrometer chip, as shown in Fig. 8(a) and (b), demonstrates the potential of this hybrid technology for chip-scale integrated spectrometers [17]. The DVS-BCB that is used as a bonding agent has an absorption spectrum as shown in Fig. 8(c). A strong absorption in the 3-3.5 μm wavelength band can be observed (due to C-H stretching vibrations). Given the compact size of these photodetectors ($\sim 20\mu\text{m}$ long), this absorption is not expected to have a substantial impact on the device responsivity even when operating at wavelengths beyond $3\mu\text{m}$.

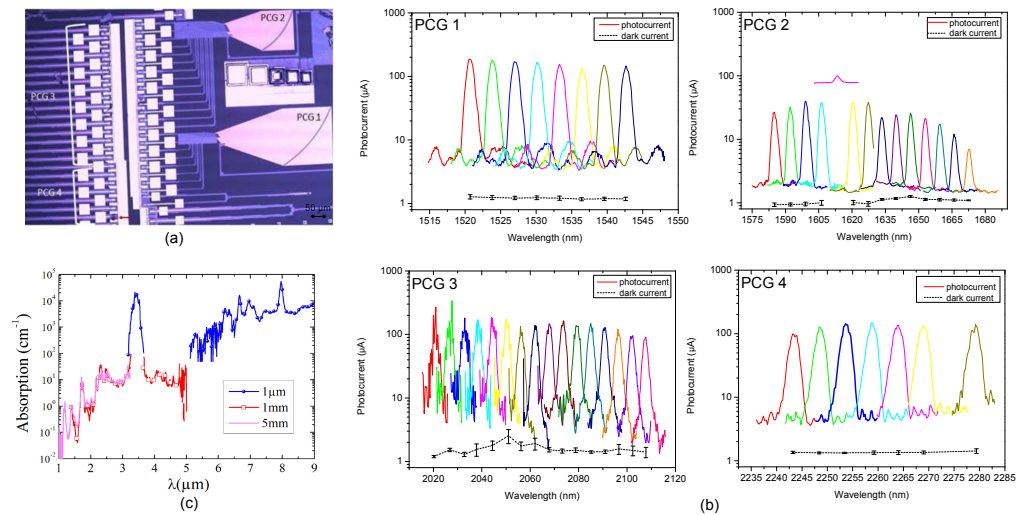


Fig. 8. (a) Microscope picture of the heterogeneously integrated photodiode array on top of a planar concave grating spectrometer; (b) representative spectral response (photocurrent versus wavelength) of the different channels of the spectrometer in different wavelength ranges covering 1500nm-2300nm; (c) DVS-BCB absorption spectrum in the mid-infrared wavelength range.

Besides GaSb photodetectors, also GaSb-on-Si laser sources are being developed. However, in this case the DVS-BCB absorption can have a substantial impact on the device performance. This problem can however be mitigated by exploiting a molecular wafer bonding process which is free of organic materials at the bonding interface [40]. In addition, direct epitaxial growth of GaSb laser structures on silicon substrates has recently been reported [43,44]. The most attractive approach for the integration of long-wavelength superlattice-based lasers such as quantum cascade and interband cascade lasers with silicon

waveguide circuits currently seems to be butt-coupling, given the fact that this provides the best heat-sinking for the laser source and the fact that – given the relatively large mode-field diameters – the alignment accuracy between both chips is relaxed. First results in that direction have recently been reported [45].

6. IV-VI colloidal quantum dot integration

While III-V semiconductor heterogeneous integration provides an interesting approach to the integration of high-quality photodetectors on a silicon waveguide circuit, the use of III-V epitaxial material has a substantial impact on the cost of the final device. Therefore, the use of a low-cost technique for photodetector integration is required. Several methods and materials can be considered for this purpose. In [46], evaporated nanocrystalline PbTe is considered as a photoconductive absorber. Amorphous InSb and InAsSb have also been considered [47]. Evaporation is however not so efficient in terms of material usage, especially when only a small fraction of the chip surface needs to have photodetectors. Graphene, with its zero bandgap and peculiar electronic and optical properties is also considered for broadband mid-infrared detectors [48]. The integration of such monolayers on silicon waveguide circuits however is still far from trivial. Our approach is based on the chemical synthesis of PbS nanoparticles in solution, which can then be applied to the silicon waveguide circuit by means of spotting (as a material-effective technique), dip coating or spin coating [49]. The optical properties of these nanoparticles is determined by their size, due to quantum confinement effects, which can be used to control the bandgap of the resulting material [50]. While these quantum dots are surrounded by organic ligands in the solution to prevent them from clustering, these ligands are to be replaced by much shorter, inorganic ligands to allow efficient current transport in the deposited quantum dot film. Recently, such a ligand exchange process was developed, leading to the demonstration of PbS-based photoconductors integrated on a silicon wafer [49,51]. A microscope image of a patterned quantum dot film on an interdigitated electrode pattern is shown in Fig. 9(a). 10 nm PbS quantum dots are used to achieve an exciton transition at wavelengths beyond 2 μm , as shown in Fig. 9(b). Given the fact that carriers can be trapped in quantum dot surface states, the exciton lifetime in these dots is large, which leads to a substantial internal gain in these devices (given by the ratio between the exciton lifetime and the carrier transit time between two electrodes). However, saturation of the trap states leads to a reduced gain at increasing input power levels. The measured responsivity under surface normal illumination of the photoconductor (at 10 V bias) with increasing input power is shown in Fig. 9(c). While the use of PbS-based quantum dots limits the operation wavelength range to about 2.5 μm , operation deeper into the infrared can be realized using e.g. HgTe quantum dot structures [49,52].

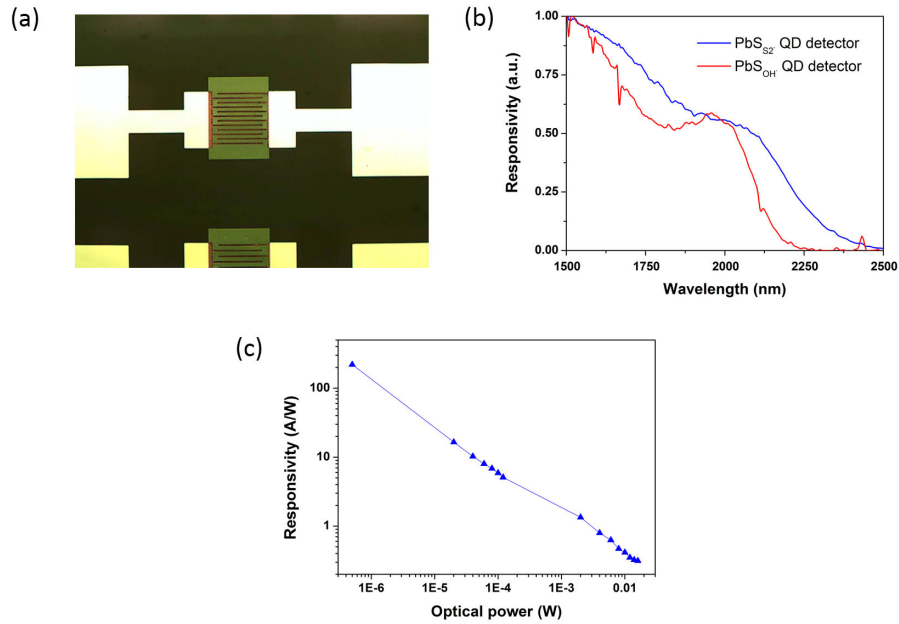


Fig. 9. (a) Microscope image of a PbS nanoparticle photoconductor integrated on a silicon wafer. (b) Absorption spectrum of the PbS nanoparticle photoconductor showing the first exciton transition of 10 nm diameter PbS nanoparticles. (c) Photoconductor responsivity as a function of optical input power

7. Conclusions

The development of silicon-based photonic integrated circuits for mid-infrared spectroscopic sensing applications is described in this paper. Both passive waveguide circuits (for linear and nonlinear applications) providing low-loss waveguides and wavelength filtering functions, as well as active functions based upon the heterogeneous integration of other materials with the silicon platform for photodetection in the mid-infrared, are reported. Besides spectroscopic sensing applications, these waveguide circuits may also find applications in next-generation telecommunication systems, which aim to exploit the large operational bandwidth of Thulium-based fiber amplifiers in the 2 μ m wavelength range for high capacity optical communication links [53].

Acknowledgements

This work was supported by the FP7-ERC-MIRACLE project, the FWO-NanoMIR project and the IWT-SBO-Glucosens project.